Spinodal dewetting in a volatile liquid film

Len M. Pismen
Department of Chemical Engineering and Minerva Center for Nonlinear Physics of Complex Systems, Technion-Israel Institute of Technology, 32000 Haifa, Israel
(Received 23 February 2004; published 9 August 2004)

The coexistence of film domains of different thickness in an evaporating film of a polar liquid on a solid substrate is studied using the multiscale expansion technique. The propagation speed of a straight-line front is computed both in the quasistationary approximation and in the comoving frame. The limit of long-scale zigzag instability is computed. The instability is observed during evaporation only and exists in a range of propagation velocities bounded both from below and from above; during condensation, the propagating front is always stable. Computations for a circular front yield a critical nucleation radius for a thin film and confirm the anomalous dependence of the evaporation rate on the droplet radius observed in recent experiments.

DOI: 10.1103/PhysRevE.70.021601 PACS number(s): 68.08.Bc, 68.15.+e, 68.03.Fg, 47.20.Ma

I. INTRODUCTION

A series of experiments by Lipson and his group has revealed complex behavior during dry-out of thin films of a polar fluid (water) on an atomically smooth mica surface [1–4]. The volatile film in contact with unsaturated vapor is bound to the substrate by both van der Waals and polar forces, which may combine to enable two alternative stable film thicknesses, both falling in a nanoscopic range. Coexisting thin and "thick" film domains have been indeed detected in the experiment. Many unusual features of pattern formation during evaporation may be attributed to the specific dynamics of boundaries between these domains.

Bistable equilibrium film thicknesses can be modeled by the Sharma potential [5] combining van der Waals and polar interactions between the fluid and substrate. Within the bistability range, the *dynamics* of a film can be described in terms of "spinodal decomposition" into two stable states. In the intermediate-thickness range, a flat interface becomes unstable. The nonlinear development of instabilities leading to nucleation of "holes" and separation into "thick" and thin domains has been studied numerically in the two-dimensional (2D) lubrication approximation [6,7] and found to follow a pattern common to many phase transition phenomena. Evaporation triggers spinodal decomposition after bringing the film thickness into the unstable range. "Dry" regions nucleating during evaporation are actually thin-film domains, and their subsequent growth can be seen as the motion of a front separating the thin- and "thick"-film domains. This relatively sharp moving front is usually identified as a "contact-line" region, although no definite equilibrium contact angle exists in the absence of a macroscopic fluid layer.

A driven contact line is apt to be unstable to transverse perturbations, which may cause fingering and rivulet formation, and are ultimately responsible for the formation of complex dewetting patterns in the course of evaporation. Such instabilities are common to contact lines driven by various forces—e.g., gravity [8–10], Marangoni force [11] or dewetting [12]—and are commonly accompanied by the formation of a ridge on the fluid interface behind the front. Transverse instability in evaporating layers was also attributed to the ridge formation [2,13]. It was conjectured that the ridge is destabilized through a mechanism analogous to the Rayleigh instability of a liquid cylinder. Numerical simulations using the common lubrication approximation [13] reproduced the zigzag instability of the front, which, indeed, appeared to be correlated, in the limited range of parameters where the simulations were carried out, with the ridge formation. Nevertheless, the connection between the instability and ridge formation, as well as the analogy to the Rayleigh instability, is open to discussion and is *not* supported by the results to be described below: we shall see that a ridge is *always* present in an evaporating film in the model we use, even when the front is stable.

Another interesting phenomenon observed in recent experiments [3,4] is the coexistence of droplets of different size, defying a common notion of faster evaporation of smaller droplets due to the Gibbs-Thomson effect. Both the anomalous dependence of the shrinkage rate on the droplet radius and the contact-line dynamics different from that observed in macroscopic films will be explained here as a consequence of the coexistence of thin- and "thick"-film domains. We shall consider the late stages of evolution of the film following spinodal decomposition and the formation of fronts. The analogy between the coexistence of domains with two alternative thicknesses and common phase transitions in 3D suggests applying the methods of the theory of phase transitions [14], based on the dynamics of propagation of the interphase boundaries. The mathematical structure of dynamic phase transition models, based on the Cahn-Hilliard equation [15], on the one side, and thin-liquid-film equations, on the other side, is not so much different, as the latter reduce in the lubrication approximation to a generalized Cahn-Hilliard equation [16–18]. A substantial difference, making the liquid-film equations technically more difficult, is in the hydrodynamic origin of the effective mobility coefficient, making it strongly dependent on the "order parameter"—film thickness (see Sec. II). This, combined with enormous disparity of scales of the bulk fluid and a "precursor layer" where molecular interactions between the fluid and substrate is predominant, presents great theoretical and computational challenges (see [18,19] for recent reviews and [20] for spe-

cific application to dewetting and spinodal decomposition in liquid films).

The dynamical problem involving a front between a thin and a "thick" film is essentially easier than that of coexistence of a thin film and macroscopic (bulk) fluid, since one can operate with nearly constant, though different, mobilities in the two domains and treat the boundary between them using the multiscale expansion technique of the dynamic theory of phase transitions [21–23]. Although the Sharma model gives a smooth transition between bistability and thin-film–bulk-fluid coexistence (see Sec. III) and has been also applied to experiments involving bulk menisci rather than coexisting domains [24], it is the bistability region where the essential features of Lipson's experiments are brought forward in a most transparent way. Applying the multiscale expansion technique allows us to solve the problem analytically for the essential symmetric shapes of the moving front separating the thin and "thick" domains. We shall use it to investigate the properties of solutions, including long-scale zigzag instability, in a wide range of parameters, as well as to give a quantitative measure of the anomalous dependence of the evaporation rate on the droplet radius.

II. BASIC EQUATIONS

The evolution equation of a *nonvolatile* liquid film with a large aspect ratio written in the lubrication approximation has the form of a generalized Cahn-Hilliard equation for the conserved "order parameter" h—the film thickness [17,18,25]. When the film thickness is indefinite, as in diffuse interface theory, it is defined as an appropriate nominal value, usually as the position of the Gibbs surface [26]. The dynamic equations follow then from the conservation law:

$$\partial_t h = -\,\boldsymbol{\nabla}\cdot\mathbf{j},\quad \mathbf{j} = -\,\eta^{-1}k(h)\,\boldsymbol{\nabla}\mu, \tag{1}$$

where $\boldsymbol{\nabla}$ is the 2D gradient operator, $\mathbf{j}$ is the flux, $k(h)$ is the effective mobility, η is dynamic viscosity, and μ is chemical potential:

$$\mu = -\,\gamma_0\nabla^2 h + \gamma'(h). \tag{2}$$

The first term in the latter expression accounts for the Gibbs-Thomson effect, γ_0 being the standard surface tension of the bulk fluid. The second term is disjoining potential, which can be defined as the derivative of the interfacial energy with respect to the film thickness, $\gamma'(h)$. We assume that there are no externally imposed forces; e.g., gravity is negligible. This form is universal for both sharp interface theories with intermolecular forces and diffuse interface theories with nominally defined h; all that varies is the form of the disjoining potential and the effective mobility $\eta^{-1}k(h)$. We shall work with the standard mobility function $k(h)=\frac{1}{3}h^3$, which corresponds to Stokes flow with no slip; possible corrections due to slip or activated creep do not change further results significantly.

If the liquid is *volatile*, the volume is not conserved, and Eq. (1) is modified to

$$\partial_t h = \eta^{-1}\,\boldsymbol{\nabla}\cdot[k(h)\,\boldsymbol{\nabla}\mu] - \beta(\mu-\mu^0), \tag{3}$$

where μ^0 is chemical potential of the ambient vapor phase and β is an effective rate constant; the effective mobility $k(h)$ remains unchanged if viscosity of the vapor phase can be neglected.

A convenient dimensionless form of Eq. (3) can be obtained by choosing a characteristic decay length d of disjoining potential (to be specified below) as the scale of film thickness h and a characteristic energy density q of molecular interactions between the fluid and substrate as the scale of chemical potential μ. The horizontal coordinates x and time can be scaled in two ways. A *short* horizontal length scale $l=\sqrt{\gamma_0 d/q}$ is fixed by the balance between disjoining potential and surface tension, and determines the extent of a region where the interface may be strongly curved due to interaction with the substrate. Another horizontal scale $L=d^{3/2}/\sqrt{\beta\eta}$ is determined by the balance between advective mass transport along the film (with $k(h)\propto d^3$) and evaporation. This scale is *long* when evaporation is slow. The respective time scales are

$$T_l = \frac{l^2\eta}{d^2 q} = \frac{\gamma_0\eta}{dq^2},\quad T_L = \frac{L^2\eta}{d^2 q} = \frac{d}{\beta q}.$$

Evolution is *quasistationary* if it proceeds on a slower time scale.

The scale ratio

$$\epsilon = \frac{l}{L} = \sqrt{\frac{T_l}{T_L}} = \frac{1}{d}\sqrt{\frac{\beta\gamma_0\eta}{q}} \tag{4}$$

is the small parameter of the problem. We shall retain the same notation for the rescaled film thickness, chemical potential, and functions of h, but to avoid confusion, distinguish between the short-scale dimensionless coordinates and time, x, t and the long-scale variables X, T, as well as between the respective gradient operators $\boldsymbol{\nabla}$ and $\hat{\boldsymbol{\nabla}}$. In scalar notation, x or X will denote coordinates normal to the front and y or Y the transverse coordinates. Using the "inner" (short) and the "outer" (long) scales, we rewrite Eq. (3) as

$$\partial_t h = \boldsymbol{\nabla}\cdot[k(h)\,\boldsymbol{\nabla}\mu] - \epsilon^2(\mu-\mu^0),\quad \mu = -\,\nabla^2 h + \gamma'(h), \tag{5}$$

$$\partial_T h = \hat{\boldsymbol{\nabla}}\cdot[k(h)\hat{\boldsymbol{\nabla}}\mu] - (\mu-\mu^0),\quad \mu = -\,\epsilon^2\hat{\nabla}^2 h + \gamma'(h). \tag{6}$$

III. STATIONARY FRONTS

Stable roots of $\gamma'(h)=\mu$, or minima of $\gamma(h)-\mu h$, correspond to stable stationary values of the film thickness. Most commonly, there is a single solution corresponding to a precursor layer. Since $\gamma'(h)=0$ at $h\to\infty$, this layer may be in equilibrium with bulk fluid at a suitable value of μ. A less common but interesting situation is the existence of more than one stable finite solutions. A suitable form of $\gamma'(h)$ is the Sharma potential [5] combining van der Waals and polar interactions:

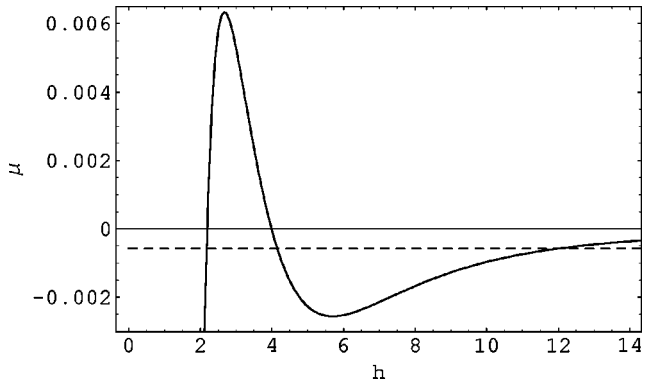

FIG. 1. The Sharma potential (8) with $\chi=0.85$. The dashed line marks the Maxwell construction level μ_s.

$$\gamma'(h) = -Q_s h^{-3} + Q_p e^{-h/d}. \tag{7}$$

The dimensionless form using d as the thickness scale and $q=Q_s/d^3$ as the energy density scale is

$$\gamma'(h) = -h^{-3} + \chi e^{-h}, \quad \chi = d^3 Q_p / Q_s. \tag{8}$$

In a certain range of the parameter χ, there are two stable roots of $\gamma'(h)=\mu$ at a fixed level of chemical potential μ (Fig. 1). Under these conditions, the liquid film may separate into domains with alternative stable values $h=h_{\pm}$. The domain boundaries are set into motion during evaporation, condensation, or coarsening. In the absence of bulk fluid, there is no asymptotic contact angle in the Young-Laplace sense, and the "droplets"—i.e., "thick" film domains—are shaped like pancakes rather than spherical caps. Both thin and "thick" films may fall into a nanoscopic range, as they indeed do in the experiments of Lipson and his group [1–4] where the ratio of the two thicknesses is of $O(10^1)$. When the liquid volume is large, both thin and thick-film domains may be in equilibrium with bulk fluid—i.e., a layer of macroscopic thickness $h\to\infty$. Although the latter is formally unstable, kinetics of rupture may be practically frozen due to negligible disjoining potential at macroscopic distances.

A straight-line stationary front separating domains with two alternative stable values $h=h_s^{\pm}$ verifies the stationary reaction-diffusion equation

$$h''(x) - \gamma'(h) + \mu = 0, \tag{9}$$

with the asymptotic conditions $h=h_s^{\pm}$ at $x\to\pm\infty$. When the liquid mass is conserved, a single planar interface cannot propagate; therefore Maxwell construction should be reached by adjusting chemical potential. The equilibrium value $\mu=\mu_s$ is obtained by multiplying Eq. (9) by $h'(x)$ and integrating across the front. The differential term vanishes upon integration, while the integral of the algebraic part yields the Maxwell condition

$$\mu_s = -\frac{\gamma(h_s^+) - \gamma(h_s^-)}{h_s^+ - h_s^-}. \tag{10}$$

This, together with $\mu_s=\gamma'(h_s^{\pm})$, defines the three unknowns μ_s, $h_s^{\pm}$. Stationary fronts exist in the interval $3(e/4)^4<\chi<e^2/8$ or, approximately, $0.6398<\chi<0.9236$.

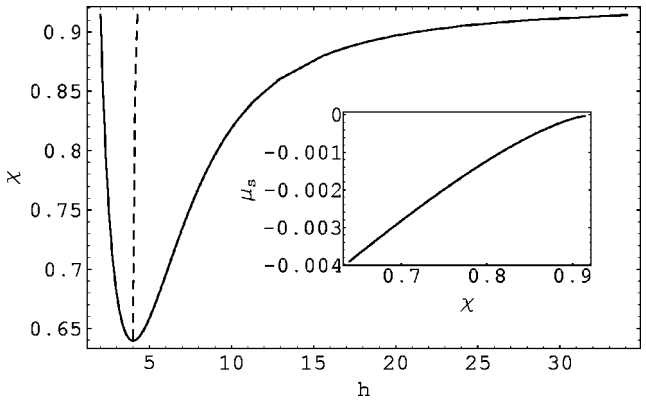

FIG. 2. Dependence of the stationary film thickness on the parameter χ. The two branches of the solid curve show the values of $h_s^{\pm}$, and the dashed line shows the intermediate unstable state h_s^0. Inset: dependence $\mu_s(\chi)$.

The alternative stationary states $h_s^{\pm}$ merge at the lower end of this interval, while at the upper end h_s^+ diverges (see Fig. 2).

The stationary front profile is computed most easily in the "phase plane" representation, using h as an independent and $p=h'(x)$ as a dependent variable. Integrating Eq. (9) yields

$$p(h) = \pm\sqrt{2}\sqrt{\gamma(h) - \gamma(h_s^-) + \mu_s(h - h_s^-)}, \tag{11}$$

and the front profile is expressed in an implicit form

$$x(h) = \frac{1}{\sqrt{2}}\int_{h_s^0}^{h} [\gamma(h) - \gamma(h_s^-) + \mu_s(h - h_s^-)]^{-1/2} dh. \tag{12}$$

The origin $x=0$ may be arbitrary, but to be definite, we have chosen it to coincide with the unstable intermediate solution h_s^0. Two typical front profiles are shown in Fig. 3. The front becomes strongly asymmetric at the upper end of the bistability interval, and its width increases, as the approach to the

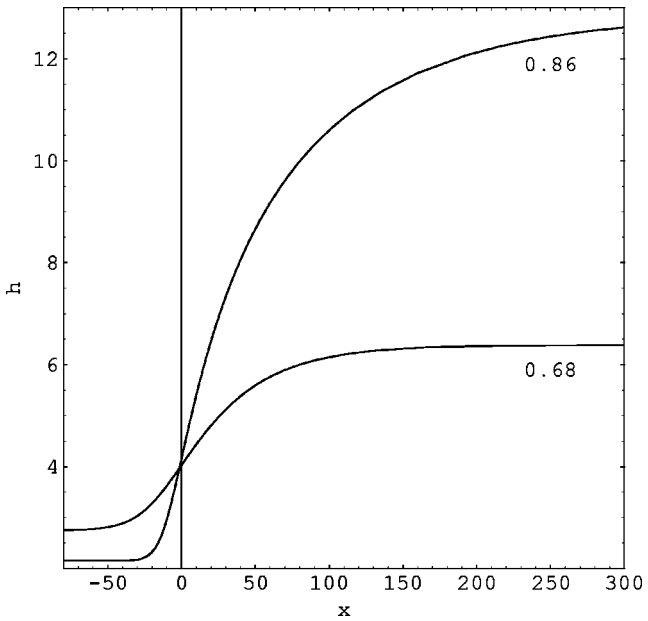

FIG. 3. The stationary front profiles for $\chi=0.86$ and $\chi=0.68$.

stationary value h_s^+ slows down at the thick side. This can be seen as a gradual crossover from the flat film to the macroscopic droplet regime at $\chi > e^2/8$. One should keep in mind that the length scale in Fig. 3 is set by the scale of molecular interactions (see Sec. II), so that the front remains narrow on the macroscopic scale even at χ not far below the limiting value. In the following, we restrict to the bistability region specific for the Sharma model and assume that the droplet size far exceeds the width of the front.

IV. INNER SOLUTION

A. Fluxes and mobility of the front

Across a narrow front, the film thickness switches between the two alternative values corresponding to the same constant value of chemical potential. The latter is constant everywhere when the two "phases" are at equilibrium, while under nonequilibrium conditions it varies on a longer $O(\epsilon^{-1})$ scale. Problems containing widely separated scales should be solved by matching expansions in the *inner* region (localized at the front) and the *outer* regions spreading out to the domains where the film thickness is almost constant. Evaporation takes place in the outer domains and can be neglected in a narrow front region. The front may be set into motion under the action of a weak gradient of chemical potential developing as a result of evaporation. The multiscale expansion approach is suitable to track slow motion of the front at times far exceeding the characteristic relaxation time T_l to a stationary front profile.

We shall allow the front to be weakly curved with a curvature radius of $O(\epsilon^{-1})$. The equations in the inner region can be written then in the *aligned comoving frame*. By convention, the x axis is directed normally to the nominal front position in such a way that the film thickness is lower to the left. The characteristic scale along this direction is the $O(1)$ short scale, while the coordinate y parallel to the front is scaled by ϵ^{-1}. We suppose that the curvature radius is of $O(\epsilon^{-1})$; then, the curvature is written as $\epsilon\kappa$ when measured on the short inner scale. The curvature is positive when the thin film domain is convex. Inasmuch as the front region is assumed to be locally at equilibrium, the front is expected to move under the influence of long-scale changes of chemical potential. Therefore the propagation speed should be measurable on a long scale L/T_L and can be written as ϵc. The chemical potential within the front region should differ from the Maxwell construction by $O(\epsilon)$ and is expressed as $\mu = \mu_s + \epsilon\mu_1$. Using this in Eq. (5) and expanding also the film thickness, $h = h_0 + \epsilon h_1 + \ldots$, we obtain, at the first order

$$\mathrm{d}_x[k(h_0)\mu_1'(x)] + ch_0'(x) = 0, \tag{13}$$

$$-\mu_1 = h_1''(x) + \kappa h_0'(x) - \gamma''(h_0)h_1. \tag{14}$$

The solutions of the inner equations should be matched at $x \to \pm\infty$ with the outer solutions, which we denote as $\mu^{\pm}(X)$, $h^{\pm}(X)$. The matching point should lie at a distance from the front that is large on the inner but small on the outer scale; the result must be independent of a precise matching position within this range.

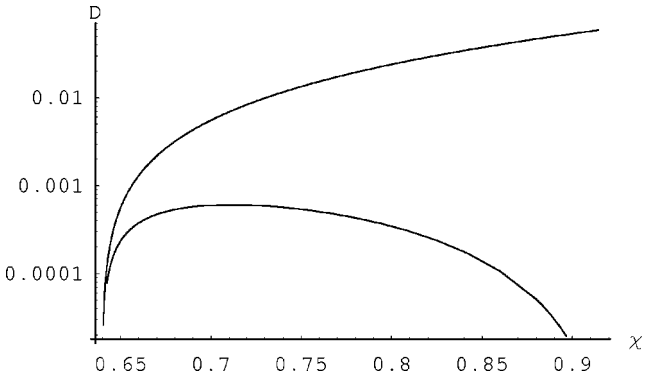

FIG. 4. Dependence of effective diffusivities in thin- (upper curve) and "thick"- (lower curve) film domains on the parameter χ.

Integrating Eq. (13) and using the matching conditions

$$\mu_1'(x) = \epsilon^{-1}\partial_x\mu^{\pm} = \boldsymbol{n}\cdot\hat{\boldsymbol{\nabla}}\mu^{\pm} \equiv -j^{\pm} \tag{15}$$

yields the material balance relation

$$c(h^+ - h^-) = -k(h^+)\boldsymbol{n}\cdot\hat{\boldsymbol{\nabla}}\mu^+ + k(h^-)\boldsymbol{n}\cdot\hat{\boldsymbol{\nabla}}\mu^- \equiv j^+ - j^-. \tag{16}$$

Here **n** is the normal to the front (directed in the same way as the x axis). The right-hand side (RHS) of Eq. (16) is the difference of the fluxes on the two sides $j^{\pm}$ driven by the gradients of chemical potential in the outer regions. This integral condition defines therefore the speed of local interface displacement required to ensure mass conservation.

Since the variable part of μ is restricted in the front region to $O(\epsilon)$, the film thickness in the matching regions may deviate from the equilibrium values $h_s^{\pm}(\mu_s)$ by no more than $O(\epsilon)$. Linearizing $\gamma'(h)$, the fluxes $j^{\pm}$ can be expressed therefore as $j^{\pm} = -D^{\pm}\mathbf{n}\cdot\hat{\boldsymbol{\nabla}}h^{\pm}$, where $D^{\pm} = k(h_s^{\pm})\gamma''(h_s^{\pm})$ are effective diffusivities. It is notable that, in spite of a strong dependence of mobility on h, the effective diffusivity turns out to be larger in the *thin*-film domain (see Fig. 4). The mass flux through the front is constant and is given by either of the equivalent expressions

$$-j_1 = ch_s^{\pm} + k(h_s^{\pm})\boldsymbol{n}\cdot\hat{\boldsymbol{\nabla}}\mu^{\pm} = ch_s^{\pm} - j^{\pm} = \frac{j^+h_s^- - j^-h_s^+}{h_s^+ - h_s^-}. \tag{17}$$

B. Solvability condition and outer limit

It remains to determine the first-order correction to the interfacial chemical potential and the related values of the film thickness $h^{\pm}$ at the matching locations on both sides of the interface. For this purpose, Eq. (13) is integrated twice to yield

$$\mu_1(x) = \overline{\mu_1} - \int_{x_0}^{x} \frac{j_1 + ch_0(x)}{k(h_0(x))}\,\mathrm{d}x. \tag{18}$$

The integration constant $\overline{\mu_1} = \mu_1(x_0)$ has to be determined by using the above expression in Eq. (14) and computing the

solvability condition of this linear inhomogeneous equation. The position x_0 is arbitrary and should fall out of the final result.

The linear operator $\mathrm{d}_x^2-\gamma''(h_0(x))$ in Eq. (14) is self-adjoint and has a zero eigenvalue corresponding to the translational Goldstone mode $h_0'(x)$. Multiplying Eq. (14) by $h_0'(x)$ and integrating yields

$$\overline{\mu_1}(h_s^+ - h_s^-) = j_1\mathcal{J}_0 + c\mathcal{J}_1 - \kappa\mathcal{I}, \tag{19}$$

where the integrals $\mathcal{I}$, $\mathcal{J}_k$ depend on the stationary front profile only:

$$\mathcal{I} = \int_{-\infty}^{\infty} [h_0'(x)]^2 \mathrm{d}x = \int_{h_s^-}^{h_s^+} p(h)\mathrm{d}h, \tag{20}$$

$$\mathcal{J}_k = \int_{-\infty}^{\infty} h_0'(x)\mathrm{d}x \int_{x_0}^{x} \frac{h_0^k(\tilde{x})}{k(h_0(\tilde{x}))}\mathrm{d}\tilde{x} = \int_{h_s^-}^{h_s^+} \mathrm{d}h \int_{h^0}^{h} \frac{\tilde{h}^k}{p(\tilde{h})k(\tilde{h})}\mathrm{d}\tilde{h}$$
$$= \int_{h^0}^{h_s^+} \frac{\tilde{h}^k(h_s^+ - \tilde{h})}{p(\tilde{h})k(\tilde{h})}\mathrm{d}\tilde{h} - \int_{h_s^-}^{h^0} \frac{\tilde{h}^k(\tilde{h} - h_s^-)}{p(\tilde{h})k(\tilde{h})}\mathrm{d}\tilde{h} \equiv \mathcal{J}_k^+ - \mathcal{J}_k^-. \tag{21}$$

The value $h^0=h(x_0)$ can be chosen to coincide with the unstable intermediate stationary solution h_s^0, but this is not necessary, as any value within the interval $h_s^-<h^0<h_s^+$ will fit as well.

The integral $\mathcal{I}$ is recognized as dimensionless line tension or energy per unit length of the front. The dependence of the excess chemical potential on curvature in Eq. (19) expresses a 2D analog of the Gibbs-Thomson relation, while the other two terms give dynamic corrections due to the flux through the interface.

The two values of chemical potential $\mu^\pm$ or film thickness $h^\pm$ to be used as interfacial boundary conditions for the outer equation are obtained by matching the outer limit of the inner solution with the inner limit of the outer solution. The limit of the inner solution (18) at $x\to\pm\infty$ is

$$\lim_{x\to\pm\infty} \mu_1(x) = \overline{\mu_1} + c\mathcal{J}_0^\pm - j^\pm\mathcal{K}^\pm + (x-x_0)\partial_x\mu^\pm, \tag{22}$$

where we have used Eq. (17) and separated the converging integrals $\mathcal{J}_0^\pm$, defined by Eq. (21), and

$$\mathcal{K}^\pm = \int_{x_0}^{\pm\infty} \left[\frac{1}{k(h_0(x))} - \frac{1}{k(h_s^\pm)}\right]\mathrm{d}x$$
$$= \int_{h_s^0}^{h_s^\pm} \frac{1}{p(h)}\left[\frac{1}{k(h)} - \frac{1}{k(h_s^\pm)}\right]\mathrm{d}h. \tag{23}$$

This formula, together with Eqs. (16), (17), and (19), yields local relations between the values of chemical potential and fluxes on both sides of the front, which can serve as the boundary conditions for outer equations. One can check by differentiating the integrals $\mathcal{J}_k^\pm$, $\mathcal{K}_\pm$ with respect to the variable limit that the limiting value of $\mu(x)$ is indeed independent of x_0 (which can be now set to zero) or h^0. The respective limits $h^\pm$ can be obtained using the near-equilibrium linearized relation

$$\mu^\pm = \mu_s + \gamma''(h_s^\pm)(h^\pm - h_s^\pm). \tag{24}$$

V. QUASISTATIONARY SOLUTIONS

A. Outer solution and matching

The film evaporates when the ambient chemical potential μ^0 drops below the prevailing chemical potential in the film—i.e. the Maxwell construction level μ_s. Evaporation taking place in the outer regions is described by Eq. (6) written in the long-scale coordinates. Assuming $\Delta\mu=\mu^0-\mu_s=O(\epsilon)$, the changes of chemical potential are restricted to $O(\epsilon)$ also in the outer domains, so that $h^\pm$ remain close to the two stationary values $h_s^\pm$. When $|\Delta_\mu|$ is sufficiently small, evaporation is slowed down to such a level that evolution is quasistationary. Then the time derivative in LHS of Eq. (6) is negligible, and it reduces, at leading order, to the inhomogeneous Helmholtz equation

$$k^\pm\hat{\nabla}^2\mu^\pm + \mu^0 - \mu^\pm = 0, \tag{25}$$

where $k^\pm=k(h_s^\pm)$. This equation has to be solved in both outer domains to find a relation between the fluxes $j^\pm$ and the values of chemical potential at the front. The problem is closed by applying the matching condition (22).

Equation (25) can be solved as a Dirichlet problem, setting $\mu^\pm(\Gamma)=\overline{\mu^\pm}$, where Γ denotes the instantaneous position of the front and $\overline{\mu^\pm}$ is as yet unknown chemical potential on either side of the front. Once the solution is found, the fluxes $j^\pm$ are computed. The chemical potential close to the front—i.e., at a distance $X\ll 1$ along the normal n to Γ, which is small on the outer scale—is computed by expanding the solution in Taylor series, and the first-order expansion should match the last term in Eq. (22). The remaining constant terms yield two matching conditions for computing $\overline{\mu^\pm}$:

$$\overline{\mu^\pm} - \mu_s = \pm j^\pm\left[\frac{\mathcal{J}_1 - h_s^\mp\mathcal{J}_0}{(h_s^+ - h_s^-)^2} + \frac{\mathcal{J}_0^\pm}{h_s^+ - h_s^-} - \mathcal{K}^\pm\right]$$
$$\mp j^\mp\frac{\mathcal{J}_1 + h_s^+\mathcal{J}_0^- - h_s^-\mathcal{J}_0^+}{(h_s^+ - h_s^-)^2} - \frac{\kappa\mathcal{I}}{h_s^+ - h_s^-}. \tag{26}$$

If the fluxes $j^\pm$ are expressed through $\overline{\mu^\pm}$ using an appropriate Green's function, Eq. (26) reduces to an integral equation defining the the local values of chemical potential. Once the fluxes on the front are known, the local propagation speed is computed with the help of Eq. (16). Successive positions of the front can be tracked by shifting it in accordance to the computed values. Following the evolution of the front in this way requires, of course, solving the integral equations at each time step. Simpler explicit solutions, which can be resolved analytically to the end, are obtained for symmetric arrangements further in this section.

B. Straight-line front

Consider a stationary solution of Eq. (25) corresponding to a straight-line front at $X=0$. The general solution is

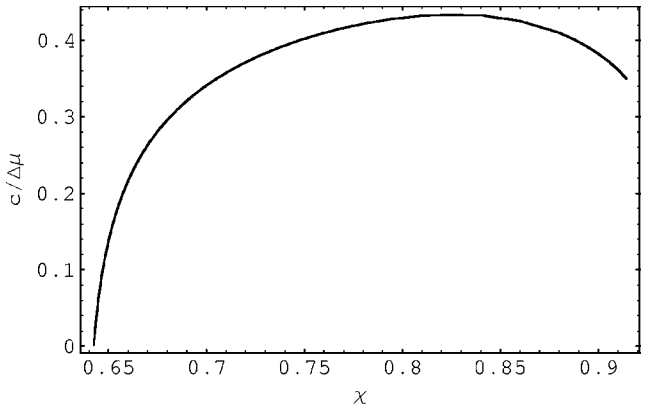

FIG. 5. Dependence of the speed of a straight-line front per unit chemical potential difference, $c/\Delta\mu$, on the parameter χ.

$$\mu^{\pm} = \mu^0 + C^{\pm} \exp(\mp X/\sqrt{k^{\pm}}). \tag{27}$$

The constants $C^{\pm}$ should be obtained by matching the inner limit of this expression with the outer limit (22) of the inner solution, where the fluxes $j^{\pm}=\pm\sqrt{k^{\pm}}C^{\pm}$ are evaluated using Eq. (27). The last term in Eq. (22) matches the first-order expansion of Eq. (27):

$$x\partial_x\mu^{\pm} = X\partial_X\mu^{\pm} = \mp C^{\pm}X/\sqrt{k^{\pm}}.$$

The remaining constant terms yield two matching conditions for computing $C^{\pm}$:

$$\Delta\mu + C^{\pm} = C^{\pm}\sqrt{k^{\pm}}\left[\frac{\mathcal{J}_1 - h_s^{\mp}\mathcal{J}_0}{(h_s^+ - h_s^-)^2} + \frac{\mathcal{J}_0^{\pm}}{h_s^+ - h_s^-} - \mathcal{K}^{\pm}\right] + C^{\mp}\sqrt{k^{\mp}}\frac{\mathcal{J}_1 + h_s^+\mathcal{J}_0^- - h_s^-\mathcal{J}_0^+}{(h_s^+ - h_s^-)^2}. \tag{28}$$

The dependence of the ratio $c/\Delta\mu$ on the parameter χ obtained by solving these two linear equations is shown in Fig. 5. The speed is positive—i.e., the thin film advances—when $\Delta\mu<0$. A slowdown at χ close to the upper limit is due to increasing capacity of the thick film. Since the equilibrium thickness decreases on the thick side when μ becomes more negative, the film profile develops a bump on the thick side during evaporation. When $\Delta\mu>0$—i.e., during condensation—the profile near the front is monotonic.

C. "Pancake" and "hole"

Circularly symmetric solutions are applicable to isolated droplets, "pancakes", or holes removed from other similar objects, as well as from any boundaries, at a distance far exceeding the characteristic horizontal scale $L=d^{3/2}/\sqrt{\beta\eta}$—i.e., unity in the long-scale dimensionless units of Eq. (25). The stationary solution of Eq. (25) corresponding to a circular thick-film "pancake" of a radius a immersed in an infinite thin layer is

$$\mu^+ = \mu^0 + C^+ I_0(r/\sqrt{k^+}),\ \mu^- = \mu^0 + C^- K_0(r/\sqrt{k^-}), \tag{29}$$

where r is the radial coordinate and I_0, K_0 are modified Bessel functions. The constants $C^{\pm}$ should be obtained in the same way as in the preceding subsection using the matching condition (28) at the front $r=a$, where one should set

$$j^+ = \sqrt{k^+}I_1(a/\sqrt{k^+}),\ j^- = -\sqrt{k^-}K_1(a/\sqrt{k^-}),\ \kappa = -a^{-1}.$$

The problem is solved analytically, but the resulting expressions are too cumbersome and the results can better assessed graphically. The front speed is expressed by a linear relation

$$c = f_0(a) + f_1(a)\Delta\mu. \tag{30}$$

The dependence of both coefficients on a is qualitatively similar for all values of χ within the bistability interval (see Fig. 6). Notably, the front speed *increases* with growing radius, in accordance to observations of Leizerson *et al.* [3,4]. The dependence is monotonic at large $|\Delta\mu|$, while at smaller $|\Delta\mu|$ the speed passes a maximum at a certain radius (see Fig. 7).

The increase of the front propagation speed means (in a limited sense) that "large droplets evaporate faster," as the title of Ref. [3] states. This is, in essence, a consequence of the "bulk" evaporation from the interior of the droplet, which has no analog in conventional evaporation of 3D droplets. The effect disappears when flux through the boundary plays a larger role in evaporation of "thick" domains. One can seen from a simple calculation that, if the evaporation rate per unit area were constant, the shrinkage rate following from the material balance would be $da/dt\propto a$. The actual

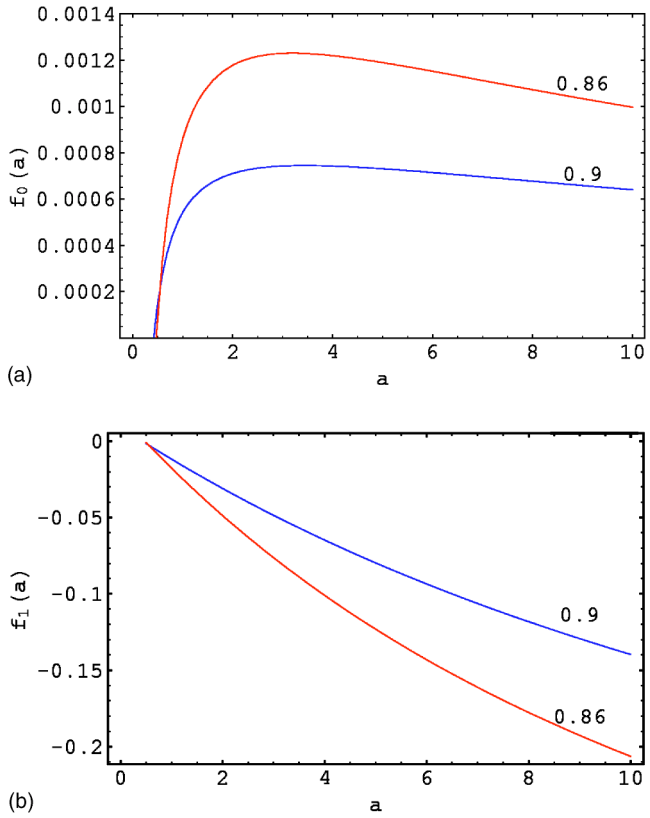

FIG. 6. The coefficients in the linear dependence (30) of the speed of the circular "pancake" boundary on the chemical potential difference at two different values of the parameter χ.

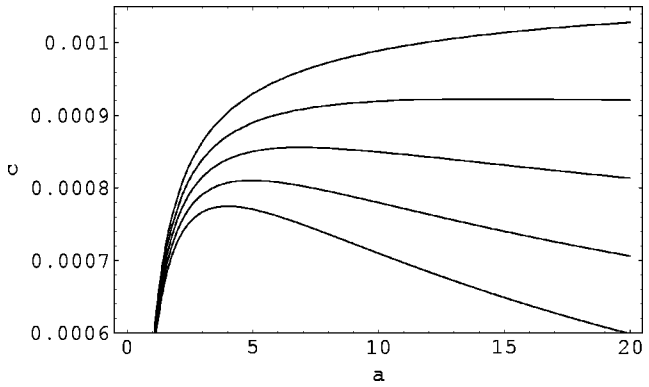

FIG. 7. The dependence of the speed of the circular boundary on the "pancake" radius at $\chi=0.9$ and different values of $\Delta\mu$. The latter change from $\Delta\mu=-0.5\times10^{-3}$ for the lower curve to $\Delta\mu=-2\times10^{-3}$ for the upper curve with the increment 0.5×10^{-3}.

radial dependence is weaker than linear, which can be attributed to slower evaporation from larger droplets, which are closer to equilibrium with the ambient vapor phase in their interior. The total evaporation time *increases* with radius, as it must do, since even a large droplet becomes small before disappearing altogether. Nevertheless, smaller droplets are less disadvantaged here than in a usual coarsening process when the front speed increases with increasing curvature.

For an opposite arrangement—a thin "hole" of a radius a immersed in an infinite thick layer—the stationary solution of Eq. (25) is

$$\mu^+ = \mu^0 + C^+K_0(r/\sqrt{k^+}),\quad \mu^- = \mu^0 + C^-I_0(r/\sqrt{k^-}). \quad (31)$$

The constants $C^\pm$ are obtained using the matching condition (28) at the front $r=a$, where one should set

$$j^+ = \sqrt{k^+}K_1(a/\sqrt{k^+}),\quad j^- = -\sqrt{k^-}I_1(a/\sqrt{k^-}),\quad \kappa = a^{-1}.$$

The coefficients in the linear dependence (30) of the propagation speed on chemical potential difference are shown in Fig. 8. The dependence of the critical radius a_c of an incipient hole nucleating during evaporation on $\Delta\mu$ is shown in Fig. 9.

VI. BEYOND QUASISTATIONARITY

A. Solution in a comoving frame

The quasistationary approximation becomes inadequate when the front propagation speed increases. Then the nonstationary equation (6) has to be solved in the outer regions. Assuming as before that $h^\pm$ remain close to the two stationary values $h_s^\pm$ and using the equilibrium relation (24), the outer equations can be rewritten as

$$[\gamma''(h^\pm)]^{-1}\partial_t\mu^\pm = k^\pm\hat{\nabla}^2\mu^\pm + \mu^0 - \mu^\pm. \quad (32)$$

For a straight-line front, this equation can be solved in the comoving frame propagating with an as yet unknown speed c. It is rewritten then as

$$\hat{c}\mu_X^\pm + k^\pm\hat{\mu}_{XX}^\pm + \mu^0 - \mu^\pm = 0, \quad (33)$$

where $\hat{c}=c/\gamma''(h_s^\pm)$. The general solution is

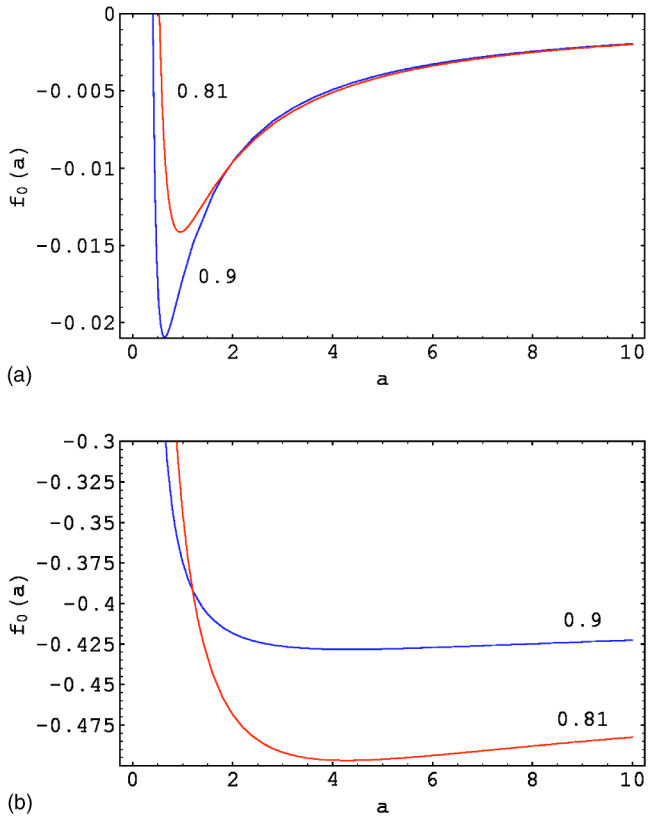

FIG. 8. The coefficients in the linear dependence (30) of the speed of the circular "hole" boundary on the chemical potential difference at two different values of the parameter χ.

$$\mu^\pm = \mu^0 + C^\pm e^{\lambda^\pm X},\quad \lambda^\pm = -\frac{\hat{c}}{2k^\pm}\left(1 \pm \sqrt{1+\frac{4k^\pm}{\hat{c}^2}}\right). \quad (34)$$

The fluxes $j^\pm=-k^\pm\lambda^\pm C^\pm$ are now velocity dependent, so that these expressions have to be solved together with Eq. (16), and the algebraic structure of the matching conditions (26) becomes very cumbersome. Fortunately, the dependence on $\Delta\mu$ remains linear, and the implicit dependence $\Delta\mu(c)$ can be obtained analytically, albeit in a form not fit for a human eye. Two typical curves are shown in Fig. 10. A graphical comparison with the quasistationary solution in the

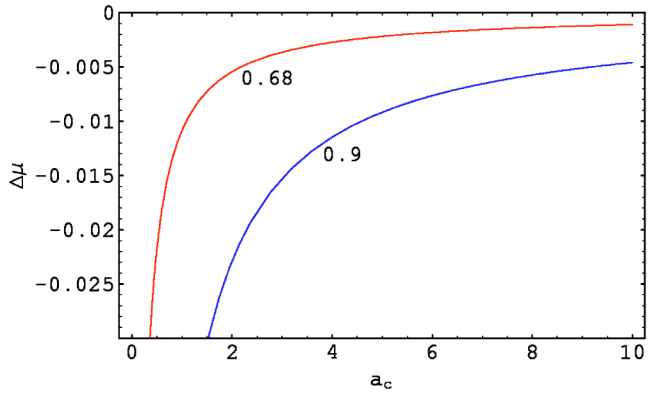

FIG. 9. The dependence of the critical radius a_c of a hole nucleating during on $\Delta\mu$ at two different values of the parameter χ.

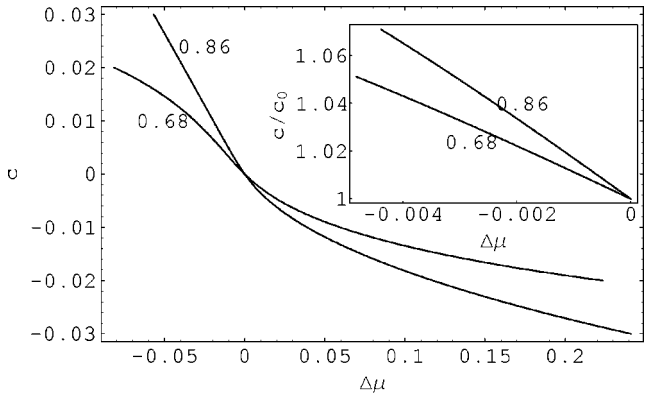

FIG. 10. The propagation speed computed in the comoving frame as a function of $\Delta\mu$ at two different values of the parameter χ. Inset: the ratio of propagation speed computed in the comoving frame to that computed in the quasistationary approximation.

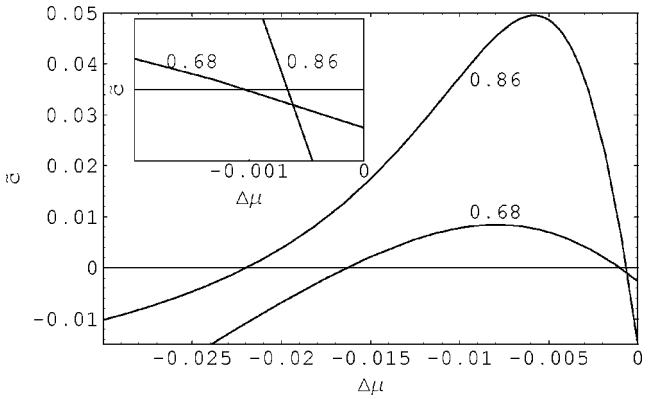

FIG. 11. The curvature correction $\tilde{c}$ to the front propagation speed computed in the comoving frame as a function of $\Delta\mu$ at two different values of the parameter χ. Inset: blowup near the origin. The front is unstable when $\tilde{c}>0$.

inset shows that the difference between the propagation speed computed in the comoving frame and that computed in the quasistationary approximation remains within a few percentage points when $\Delta\mu$ is within the same range as the difference between μ_s and the equilibrium chemical potential for the bulk fluid. This can serve as an indication of reliability of the above results for the "pancake" and "hole" configurations, which do not admit a comoving formulation of the outer problem and leave full dynamic simulation as the only alternative to the quasistationary solution.

The nonlinear character of the $c(\Delta\mu)$ dependence, which is characteristic to the comoving frame computations, becomes qualitatively important at high speeds. There is a maximum propagation speed at $\Delta\mu<0$, but it is achieved at very high potential differences, far beyond the instability threshold to be computed in the next subsection. The nonlinearities are interrelated with changes in the flux through the interface j_1. At relevant small propagation speeds, up to and beyond the instability limit, the flux is directed during evaporation towards the thin-film domain, implying a higher efficiency of evaporation in the thin layer.

B. Zigzag instability

A straight-line front may become unstable to transverse perturbations. Since the front is neutrally stable to translations, the onset of instability is most likely to occur in a *long-scale* mode. We consider a straight-line front parametrized by the coordinate Y and denote the instantaneous displacement of the front from its unperturbed position along the X axis directed towards the region occupied by the thick film as $\zeta(Y,T)$. The inner front solution is assumed to remain quasistationary, while instability is developing or decaying in the outer domains; therefore the outer (long) scale is suitable for stability analysis. As long as the amplitude of the perturbation is much smaller than its wavelength, the normal vector defining the direction of the front propagation is almost parallel to the X axis and the propagation speed is expressed as $\zeta_T=c$. In the same approximation, the curvature is given by $\kappa=-\zeta_{YY}$.

The long-scale instability can be studied in the comoving frame using Eq. (33) corrected by taking into account front curvature, which is assumed to be small *even on the extended scale*:

$$\hat{c}\mu_X^{\pm}+k^{\pm}(\hat{\mu}_{XX}^{\pm}-\kappa\mu^{\pm})+\mu^0-\mu^{\pm}=0. \tag{35}$$

The local front propagation speed, as well as $\mu^{\pm}$ and $j^{\pm}$, is expanded in $\kappa\ll 1$. The curvature correction to the front propagation speed is presented as $c=c_0+\tilde{c}\kappa$, where c_0 is the speed of a straight-line front evaluated in the preceding subsection. The first-order correction $\tilde{c}$ is computed by using the first-order solution of Eq. (35) in the matching conditions at the front (16) and (26) expanded likewise to the first order in κ. The problem is solved analytically along the same lines as in the preceding subsection, producing awesome expressions handled by computer algebra.

The front is unstable when the curvature correction $\tilde{c}$ is positive. The instability is observed at $\Delta\mu<0$ (i.e., during evaporation) in an interval limited both from below and from above; at $\Delta\mu>0$ (condensation) the front is always stable. The curves $\tilde{c}(\Delta\mu)$ for two chosen values of χ are shown in Fig. 11. The onset of instability is observed at rather low propagation speeds, and the front stabilizes again at higher speeds or $|\Delta\mu|$, as, apparently, perturbations are swept under by the propagating front. It is possible, however, that other instabilities, which we do not investigate here, become relevant at high speeds. The values of $|\Delta\mu|$ and c_0 at the lower limit of zigzag instability are plotted as functions of χ in Fig. 12. A full dispersion relation, including both transverse instabilities at finite wavelength and oscillatory instabilities, can be obtained using the same approach as described above, but rather extensive computations are needed to determine the instability limits.

VII. CONCLUSIONS

The above theory is more similar technically to the macroscopic dynamic theory of phase transitions than to a common description of thin fluid films. Although the background equations providing the physical basis of mobility are of hy-

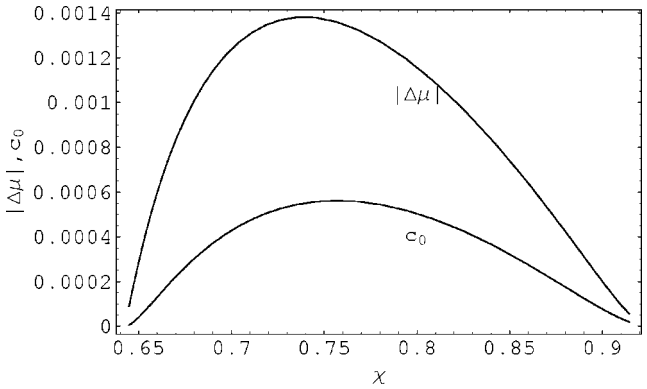

FIG. 12. The values of the chemical potential difference $|\Delta\mu|$ and propagation speed of the straight-line front c_0 at the lower limit of zigzag instability as functions of χ.

drodynamic origin, the dynamics is defined here in terms of motion of a relatively sharp "interphase" boundary (front) separating the two alternative thermodynamically stable states of the film. The dynamic phase transition theory, though providing the basic methods, cannot guide intuition in this problem, where the dynamics strongly depends on the presence of "bulk" evaporation from the interior of thin and "thick" domains and the disparity of mobility coefficients and effective diffusivities.

Our ability to solve the problem analytically with the help of the multiscale perturbation technique helps us to investigate a far wider range of conditions than would be accessible for numerical simulations, though due to the nature of the problem, all expressions are inevitably cumbersome and the solution has to be computer aided both at derivation and assessment stage.

Two principal results have to emphasized here. First, the anomalous dependence of the propagation speed on the curvature of the boundary between thin and "thick" domains, which, in accordance to the experiment [3,4], depresses coarsening of the droplet size distribution. Second, the nature of zigzag instability, which bears more similarity to Mullins-Sekerka [14] rather than Rayleigh instability and is not linked to the formation of a "ridge," inevitably present during evaporation both under stable and unstable conditions. Since no ridge exists during condensation, the ridge formation can be viewed as a necessary but not sufficient condition for instability. More studies are needed to investigate a crossover from the "two-phase" behavior studied here to dynamics of a contact line between a thin precursor and a macroscopic fluid layer, but the "two-phase" model appears to express in the most clear form the specific features of the experiments of Lipson and his group.

ACKNOWLEDGMENTS

This work has been supported by the Israel Science Foundation. The author acknowledges stimulating discussions with Steve Lipson and hospitality of MPI for Physics of Complex Systems (Dresden) where a significant part of this work was carried out.

[1] M. Elbaum and S.G. Lipson, Phys. Rev. Lett. **72**, 3562 (1994).
[2] N. Samid-Merzel, S.G. Lipson, and D.S. Tannhauser, Phys. Rev. E **57**, 2906 (1998).
[3] I. Leizerson, S.G. Lipson, and A.V. Lyushnin, Nature (London) **422**, 395 (2003).
[4] I. Leizerson, S.G. Lipson, and A.V. Lyushnin, Phys. Rev. E **68**, 051601 (2003)
[5] A. Sharma, Langmuir **9**, 3580 (1993).
[6] A. Sharma, Langmuir **14**, 4915 (1998).
[7] A.S. Padmakar, K. Kargupta, and A. Sharma, J. Chem. Phys. **110**, 1735 (1999).
[8] J.R. de Bruyn, Phys. Rev. A **46**, R4500 (1992).
[9] A.L. Bertozzi and M.P. Brenner, Phys. Fluids **9**, 530 (1997).
[10] Y. Ye and H.-C. Chang, Phys. Fluids **11**, 2494 (1999).
[11] A.A. Golovin, B.Y. Rubinstein, and L.M. Pismen, Langmuir **17**, 3930 (2001).
[12] G. Reiter and A. Sharma, Phys. Rev. Lett. **87**, 166103 (2001).
[13] A.V. Lyushnin, A.A. Golovin, and L.M. Pismen, Phys. Rev. E **65**, 021602 (2002).
[14] J.S. Langer, Rev. Mod. Phys. **52**, 1 (1980).
[15] J.W. Cahn and J.E. Hilliard, J. Chem. Phys. **28**, 258 (1958).
[16] V.S. Mitlin, J. Colloid Interface Sci. **156**, 491 (1993).
[17] L.M. Pismen and Y. Pomeau, Phys. Rev. E **62**, 2480 (2000).
[18] L.M. Pismen, Colloids Surf., A **206**, 11 (2002).
[19] Y. Pomeau, C. R. Mec. **330**, 207 (2002).
[20] U. Thiele, M.G. Velarde, K. Neuffer, M. Bestehorn, and Y. Pomeau, Phys. Rev. E **64**, 061601 (2001).
[21] R.L. Pego, Proc. R. Soc. London, Ser. A **422**, 261 (1989).
[22] G. Caginalp, Phys. Rev. A **39**, 5887 (1989).
[23] A. Karma and W.-J. Rappel, Phys. Rev. E **57**, 4323 (1998).
[24] S.J. Gokhale, J.L. Plawsky, and P.C. Wayner, J. Colloid Interface Sci. **259**, 354 (2003).
[25] A. Oron, S.G. Bankoff, and S.H. Davis, Rev. Mod. Phys. **69**, 931 (1997).
[26] L.M. Pismen, Phys. Rev. E **64**, 021603 (2001).